Research Paper

Water-Soluble Phthalocyanines Selectively Bind to Albumin Dimers: A Green Approach Toward Enhancing Tumor-Targeted Photodynamic Therapy

Xingshu Li[1,2#], Keunsoo Jeong[3#], Yoonji Lee[4#], Tian Guo[2], Dayoung Lee[2], Jeongmin Park[3], Nahyun Kwon[2], Jung-Hyun Na[2], Seung Kon Hong[2], Sun-Shin Cha[2], Jian-Dong Huang[1✉], Sun Choi[4✉], Sehoon Kim[3,5✉], and Juyoung Yoon[2✉]

1. College of Chemistry, State Key Laboratory of Photocatalysis on Energy and Environment, Fujian Provincial Key Laboratory of Cancer Metastasis Chemoprevention and Chemotherapy, Fuzhou University, Fuzhou 350108, China.
2. Department of Chemistry and Nano Science, Ewha Womans University, Seoul 03760, Republic of Korea.
3. Center for Theragnosis, Korea Institute of Science and Technology (KIST), Seoul 02792, Republic of Korea.
4. College of Pharmacy and Graduate School of Pharmaceutical Sciences, Ewha Womans University, Seoul 03760, Republic of Korea.
5. KU-KIST Graduate School of Converging Science and Technology, Korea University, Seoul 02841, Republic of Korea.

#These authors contributed equally to this work.

✉ Corresponding authors: jdhuang@fzu.edu.cn (J.D.H.); sunchoi@ewha.ac.kr (S.C.); sehoonkim@kist.re.kr (S.K.); jyoon@ewha.ac.kr (J.Y.).

Abstract

Targeted delivery of therapeutic agents is of particular interest in the field of cancer treatment. However, there is an urgent need for developing clinically promising targeting approaches that can be readily administered in a green manner.

Methods: Five phthalocyanine derivatives bearing different anionic and cationic groups were designed and synthesized. Then, their binding affinity with albumin were studied using gel assays, optical spectra and computational simulation. Finally, *in vitro* and *in vivo* fluorescence imaging and photodynamic therapy (PDT) evaluations were carried out.

Results: The two positively charged compounds could selectively bind to albumin dimer over albumin monomer, while the three negatively charged phthalocyanines could bind to both albumin monomer and dimer. Following systemic administration, the phthalocyanines show improved tumor accumulation via transport by natural albumin. PDT evaluations indicate that one of the positively charged compounds, $ZnPcN_4$, shows outstanding phototherapeutic efficacy against tumors in preclinical models.

Conclusion: Our findings demonstrate that the use of water-soluble phthalocyanines as photosensitizers and *in vivo* albumin as a natural carrier may provide a green and efficient approach for tumor-targeted imaging and therapy.

Key words: photodynamic therapy, phthalocyanine, albumin dimer, natural carrier, tumor targeting

Introduction

Targeted therapy, which delivers the right therapeutic agents to the right target to efficiently achieve localized control of the tumor with minimal side effects, is a highly promising cancer therapeutic strategy [1-5]. However, there is an urgent need to develop clinically relevant targeting approaches that can be readily administered in a green manner.

Albumin, the most abundant protein in the blood, is closely related to the regulation of plasma colloid osmotic pressure and the transport of numerous endogenous and exogenous compounds [6,7]. Many studies have claimed that albumin is most

likely involved in the provision of nutrition to tumors [8]. Albumin receptors that are overexpressed on cancer cells, such as glycoprotein 60 and the albumin-binding protein SPARC (secreted protein acidic and rich in cysteine), have been found to facilitate the accumulation, distribution and degradation of albumin in tumor tissues [6,9,10]. Owing to its potential for enhanced permeability and retention (EPR) effect, albumin has been extensively explored as a versatile nanocarrier for drug delivery via covalent conjugation and noncovalent interactions [6,7,11-16]. However, most of the existing albumin-based delivery systems utilize *in vitro* albumins and even require extra materials to construct and stabilize these systems. These albumin-based platforms suffer from certain shortcomings, including tedious fabrication, poor reproducibility, the potential immunogenicity of *in vitro* albumin and the potential toxicity of system complexes, which hamper their future clinical translation. In contrast, we herein demonstrate a green tumor-targeting approach using *in vivo* albumin as a carrier for delivering molecular dye-based photosensitizers.

Zinc(II) phthalocyanines are photosensitizers with high potential for photodynamic therapy (PDT) due to their strong absorption in the far-red/near-infrared regions and high efficiency in generating reactive oxygen species (ROS) [17-21]. Recently, several studies reported that zinc(II) phthalocyanines substituted with hydrophilic groups (*e.g.*, carboxyl and sulfonic acids) show strong binding affinity with albumin [22-24]. Inspired by these reports, we herein attempt to utilize this binding affinity to provide a new approach for targeted PDT. In addition, to systematically study the interaction mechanism between albumin and phthalocyanine molecules, phthalocyanine derivatives bearing different anionic and cationic groups are designed and synthesized (**Figure 1**). Interestingly, we find that all of these water-soluble phthalocyanines can specifically bind to albumin, which in turn enhances their tumor-targeting ability. In particular, the positively charged phthalocyanines selectively bind to albumin dimer over albumin monomer, and the phthalocyanine bearing four cationic groups (ZnPcN$_4$) shows outstanding PDT efficacy against tumors in preclinical models.
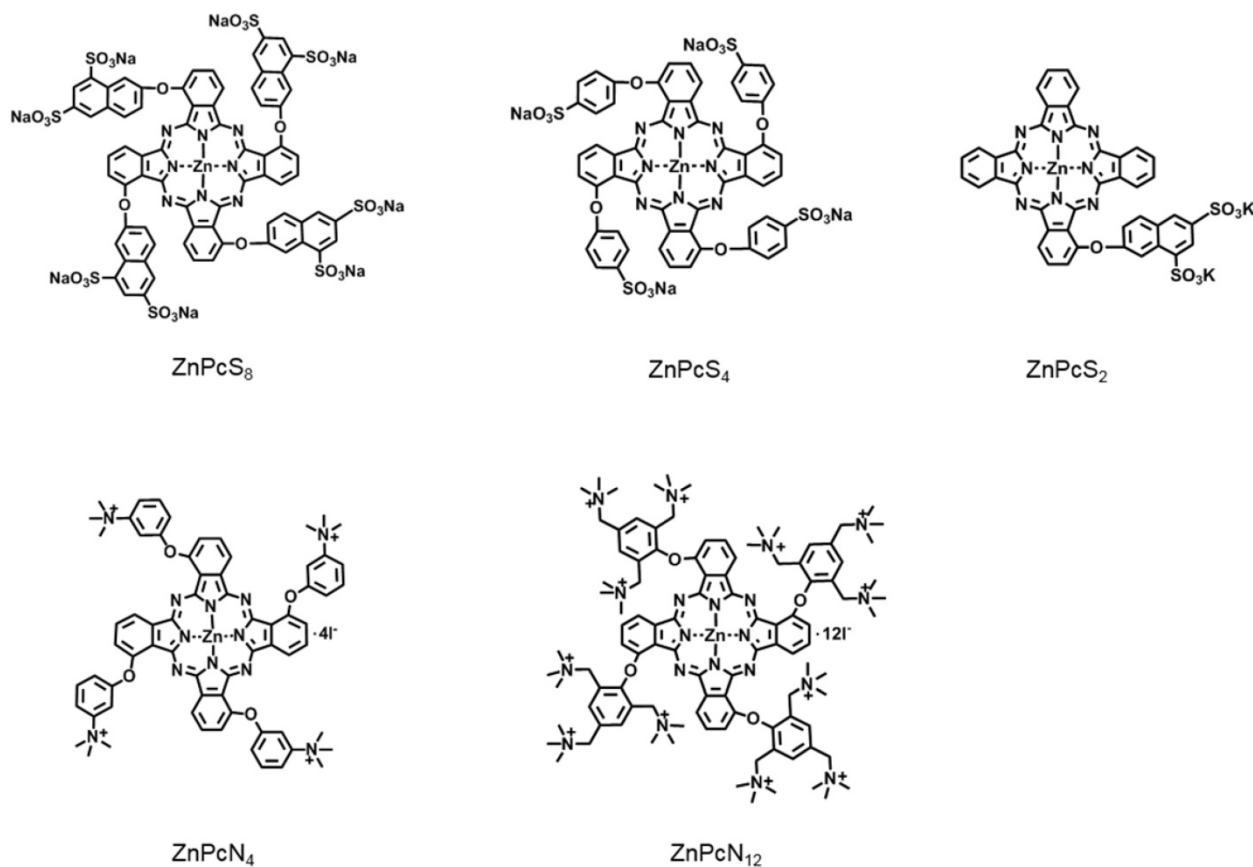

Figure 1. Chemical structures of the phthalocyanines, including ZnPcS$_8$, ZnPcS$_4$, ZnPcS$_2$, ZnPcN$_4$, and ZnPcN$_{12}$. Here, only one of the possible C$_{4h}$ isomers is displayed for the tetrasubstituted phthalocyanines.
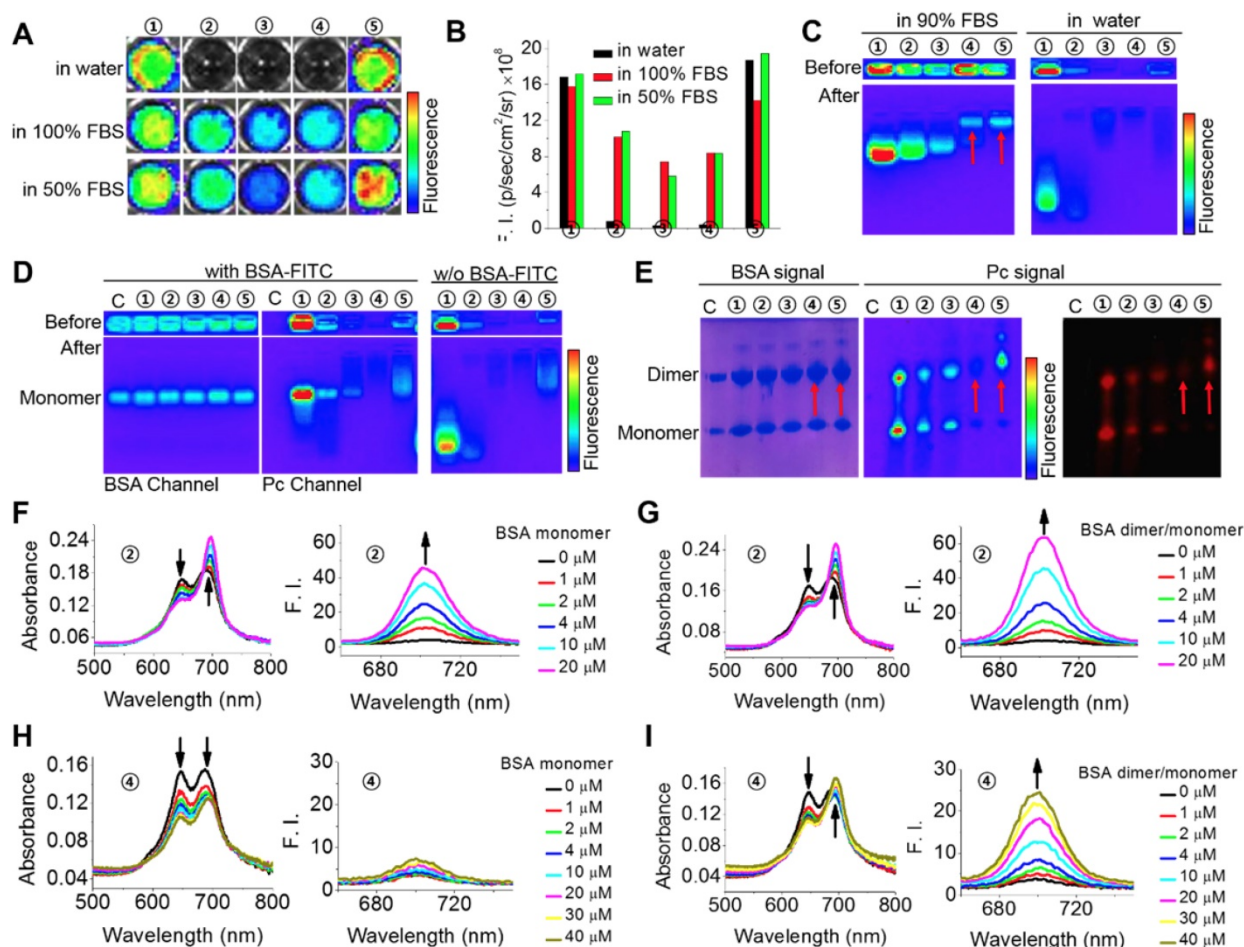
Figure 2. Specific interactions between the phthalocyanines and albumin monomer or dimer. (A-B) Fluorescence images (A) and fluorescence intensities (B) of the phthalocyanines in aqueous solutions containing 0, 50, and 100% FBS. ①: ZnPcS$_8$. ②: ZnPcS$_4$. ③: ZnPcS$_2$. ④: ZnPcN$_4$. ⑤: ZnPcN$_{12}$. All the compounds were at 20 μM. The images were obtained when the solutions had stood for 5 min after phthalocyanine dissolution in the media. Fluorescence images were excited at 640 nm and monitored at 720 nm with an IVIS Lumina II imaging system. (C) Gel assays of phthalocyanines in water with and without FBS. All the phthalocyanines were at 2 μM. Gel: 2% agarose gel. Running conditions: 100 V, 20 min. (D) Gel assays of phthalocyanines in PBS with and without BSA monomer (18 μM, labeled with FITC). All the phthalocyanines were at 2 μM. Gel: 2% agarose gel. Running conditions: 100 V, 20 min. FITC was excited at 430 nm and monitored at 520 nm. Phthalocyanines were excited at 640 nm and monitored at 720 nm. C: control, without any phthalocyanine. (E) Native polyacrylamide gel electrophoresis (PAGE) of the phthalocyanines with albumin in PBS (pH 7.4). The gel was stained with Coomassie brilliant blue (CBB) to indicate albumin monomer (~66 kDa) and dimer (~132 kDa) and imaged in both the CBB and phthalocyanine channels. The red arrows indicate the locations of both albumin dimer and ZnPcN$_4$ or ZnPN$_{12}$. (F) Absorption and fluorescence spectra of ZnPcS$_4$ (2 μM) in water with different concentrations of BSA monomer. (G) Absorption and fluorescence spectra of ZnPcS$_4$ (2 μM) in water with different concentrations of BSA dimer/monomer. (H) Absorption and fluorescence spectra of ZnPcN$_4$ (2 μM) in water with different concentrations of BSA monomer. (I) Absorption and fluorescence spectra of ZnPcN$_4$ (2 μM) in water with different concentrations of BSA dimer/monomer.

Results and Discussion

Phthalocyanines selectively bind to albumin

To investigate the possible interaction of the phthalocyanines with proteins, we first compared their different fluorescence profiles in pure water and protein-containing solutions. As shown in **Figure 2A-B**, fetal bovine serum (FBS) could obviously enhance the fluorescent intensities of ZnPcS$_4$, ZnPcS$_2$ and ZnPcN$_4$ but caused almost no changes in those of ZnPcS$_8$ and ZnPcN$_{12}$. This difference is probably because of their different states in aqueous solution. ZnPcS$_8$ and ZnPcN$_{12}$ molecules have enough electrostatic repulsion between them to prevent aggregation-induced quenching. As a result, they already show strong fluorescence emission in pure water. In contrast, ZnPcS$_4$, ZnPcS$_2$ and ZnPcN$_4$ form

aggregates in pure water, which may be reduced upon adding FBS. To determine which protein may be involved in these interactions, gel assays and mass analysis were carried out. The results indicated that ZnPcS$_8$, ZnPcS$_4$ and ZnPcS$_2$ most likely bind to the albumin monomer, while ZnPcN$_4$ and ZnPcN$_{12}$ most likely bind to the albumin dimer (**Figure 2C** and **Figure S1**). To confirm their binding with the albumin monomer or dimer, pure bovine serum albumin (BSA) monomer and a BSA monomer/dimer (3/7) mixture were utilized for further studies. As shown in **Figure 2D-E**, gel assays confirm that ZnPcS$_8$, ZnPcS$_4$ and ZnPcS$_2$ can bind to both albumin monomer and dimer, while ZnPcN$_4$ and ZnPcN$_{12}$ can bind to only albumin dimer. In addition, the results of absorption and fluorescence spectral measurements confirm that both pure BSA monomer and the BSA

monomer/dimer mixture can reduce the ZnPcS$_4$ aggregates, while only BSA dimer can reduce the ZnPcN$_4$ aggregates (**Figure 2F-I**). These results indicate that all five of these phthalocyanines can selectively bind to albumin over other proteins, but only the positively changed compounds (ZnPcN$_4$ and ZnPcN$_{12}$) can selectively bind to albumin dimer over albumin monomer. It's also worth to mention that the ROS generation of the phthalocyanines could be increased after binding to albumin (**Figure S2**).

To further investigate the binding mechanism of the compounds, we carried out docking studies, in which their binding conformations to the whole structure of serum albumin were rigorously searched (see Experimental procedures and supporting **Figure S3-4**). We utilized the X-ray crystal structure of human serum albumin (HSA) bound to a heme molecule, which has a similar structural scaffold to that of our compounds (note that for BSA, the appropriate structure for the docking of comparatively large molecules such as ours is not available). Since BSA and HSA show strong similarities in their structures (sequence identity of ~75%, RSMD of ~1 Å) [25], the binding modes in both proteins might be similar. Our results showed that the compound ZnPcS$_2$ displayed two different possible binding modes: one bound at the heme binding site with the lowest energy score (**Figure 3A**) and the other bound at the cleft region (**Figure 3B**). At the heme site, the flat phthalocyanine-zinc ring nicely occupies the binding pocket, similar to the scaffold of the heme molecule, and the Zn atom coordinates with the oxygen atom of the Y161 residue. The phthalocyanine-zinc ring also forms a π-stacking interaction with Y138. The linker oxygen atom forms an ionic interaction with K190, and the two sulfonate groups interact with the K519, R114, and R186 residues. The second possible binding mode is the most highly populated conformer and is found in the cleft region, forming a dative bond with D187. The flat phthalocyanine-zinc ring penetrates the cleft site, and the two sulfonate groups establish ionic interactions with K195 and K436.

In the case of ZnPcS$_4$, the four bulky substituents make it very difficult for the compound to bind at the heme site. In particular, the heme site located in the D$_I$ domain has two disulfide bridges maintaining the structural stability of the helices. Indeed, the structural alignment of the heme site of various albumin structures showed that their architecture is very similar in all structures, suggesting that this region is not highly flexible upon binding various drugs or lipids. Although we consider protein flexibility, it seems to be nearly impossible for the tetrasubstituted phthalocyanine compounds to bind

at the heme site. Rather, they showed the lowest energy and most highly populated conformations in the cleft region (**Figure 3C**). Similar to the second binding mode of ZnPcS$_2$, this binding mode of ZnPcS$_4$ involves the flat phthalocyanine-zinc ring penetrating the cleft site and the Zn atom coordinating with D187. The sulfonate groups of the tetrasubstituted compound form ionic interactions with the surrounding positively charged residues, such as R114, K190, K195, R197, and R428. The distance between the compound's sulfonate oxygen atom and the side chain of W214 (which is the only tryptophan residue of HSA) is ~1.2 nm in the cleft binding complex and ~ 2.6 nm in the heme site binding complex (**Figure S5**). Considering that the typical range of the distance between the acceptor and the donor in fluorescence resonance energy transfer (FRET) is 1 ~ 10 nm [26], both predicted binding modes seem to be reasonable for the fluorescence quenching of the tryptophan in albumin induced by the addition of these phthalocyanines through FRET (**Figure S6**).

The scaffold of ZnPcN$_4$ can be similarly fitted to the cleft region, maintaining coordination with D187; however, its positively charged substituents seem to be electrostatically repulsed by the cleft surface (**Figure S7**; note that the electrostatic potential of the cleft region is quite positively charged and that the negatively charged region in the cleft is around the D187 residue, which coordinates with the Zn atom of our compound). This behavior may explain why, in contrast to the negatively charged compounds, which show good electrostatic complementarity to the cleft region, the positively charged compounds cannot bind well to the albumin monomer.

As shown in **Figure 2E**, ZnPcN$_4$ and ZnPcN$_{12}$ prefer to bind to the dimer structure, while the negatively charged compounds can bind to both monomer and dimer. It is well known that albumin can form a dimer. In the natural state, albumin exists in equilibrium between the monomer and dimer/oligomer [27]. Several studies have reported that increased concentrations of albumin dimer in circulating blood are associated with diseases such as chronic renal disease and oxidative damage in the blood [28-31]. However, their association mechanism has not yet been clearly identified. Among the available structural information, we selected the X-ray crystal structure of HSA dimer with the relevant interface contact (PDB id: 3JQZ).[32] This structure is complexed with lidocaine, a positively charged molecule as our compounds. Interestingly, this cationic drug molecule also occupies the cleft of HSA, and the positively charged amine group interacts with D187, which is shown in our model as the residue

coordinating with the zinc atom. Based on this crystal structure, a model of the HSA dimer bound to ZnPcN$_4$ was constructed and refined using energy minimization and Monte Carlo (MC) sampling (see Experimental procedures). As shown in **Figure 3D-E**, in addition to the interactions with the monomer, the positively charged substituents of ZnPcN$_4$ also form ionic interactions with two glutamate residues (E82 and E505) in the dimer partner. Moreover, the contact interface of the dimer partner is slightly negatively charged, so positively charged compounds can be energetically stable when they bind to the dimer structure.

Collectively, these five phthalocyanines can bind to the HSA cleft region via coordination of their Zn

atoms with D187, but the binding mechanisms of negatively and positively charged compounds are quite different. ZnPcS$_4$ binds to the monomer with its negatively charged substituents fitting very well to the cleft surface. ZnPcS$_4$ can also bind to the dimer, but direct interaction with the dimer partner seems to be negligible. While ZnPcN$_4$ can be fitted to the monomer cleft region, the positively charged substituents can be electrostatically repulsed by the surface. In the dimer structure, ZnPcN$_4$ can form ionic interactions with the dimer partner, which may contribute to the more stable and preferable binding of this compound to the dimer.
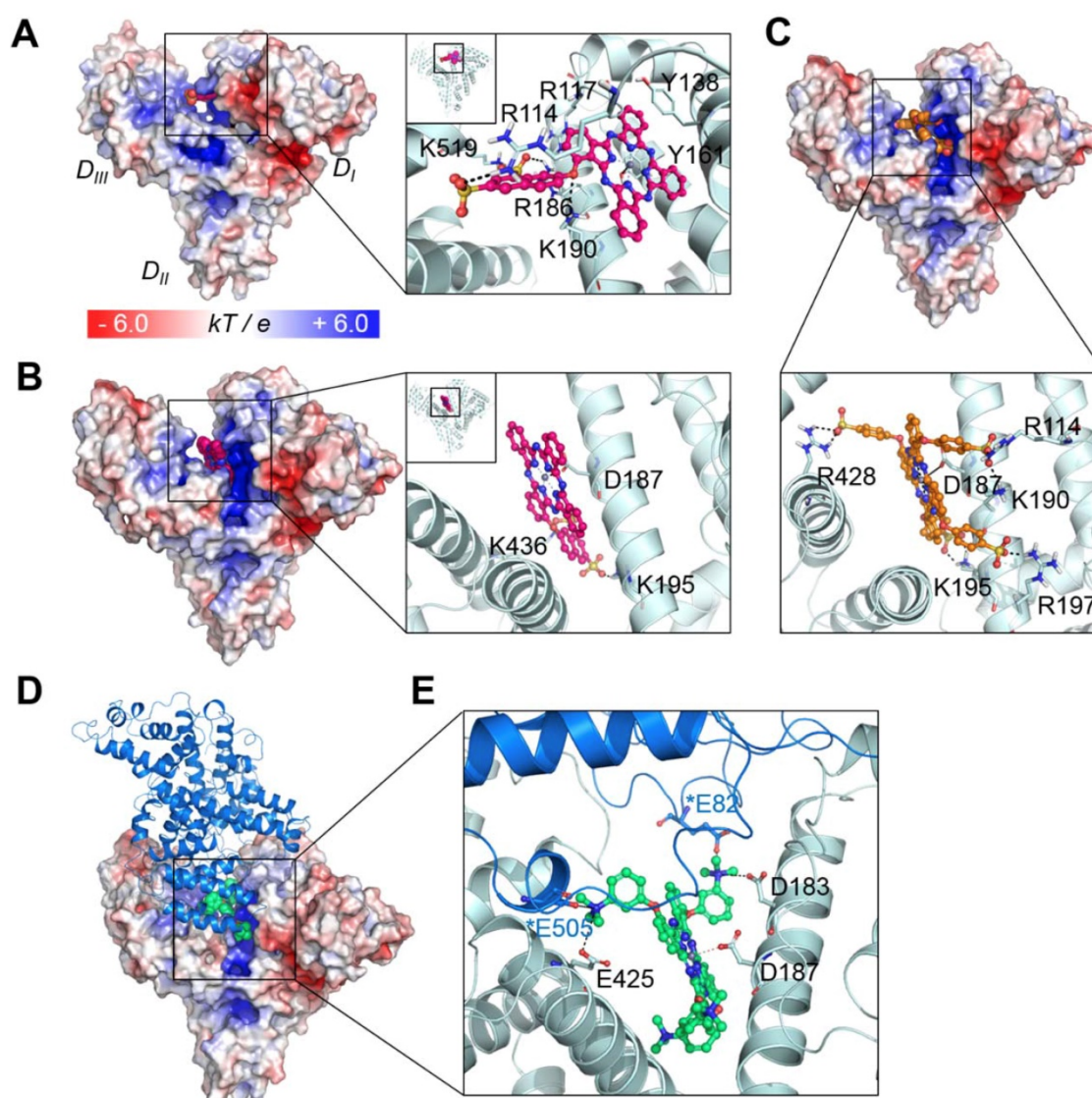

Figure 3. Binding modes of the phthalocyanines with HSA. (A) Binding mode of ZnPcS$_2$ at the heme binding site. (B) The other possible binding mode of ZnPcS$_2$ at the cleft region of HSA. (C) Binding mode of ZnPcS$_4$. The protein surface is colored by the electrostatic potential, and the bound compound is shown as spheres with the carbon atoms in magenta. In the enlarged view, the compound is displayed as a ball-and-stick model, and the interacting residues are displayed as thin sticks with their carbon atoms in light blue. The dative bond between the Zn atom and Y161 or D187 is depicted as a black line, and ionic interactions are marked by black dashed lines. (D) ZnPcN$_4$ bound at the HSA dimer interface. The protein surface of one monomer is colored by the electrostatic potential, and the bound compound is shown as spheres with the carbon atoms in lime green. The other monomer is displayed as the marine-colored ribbon. (E) The bound ZnPcN$_4$ (lime green, ball-and-stick) is coordinated to D187 via its Zn atom, and the positively charged amine substituents can form ionic interactions with several negatively charged residues (thin sticks, light blue for one monomer and marine for the dimer partner). The interacting residues in the dimer partner are marked by asterisks.

In vivo albumin as a natural carrier that enhances the tumor-targeted delivery of phthalocyanines

As introduced above, *in vitro*-processed albumin has been widely used to construct carrier systems for drug delivery. Since our phthalocyanines show strong binding affinities for albumin, we thus hypothesized that upon *in vivo* administration, they bind to endogenous albumin molecules spontaneously to form an *in situ* delivery system where albumin serves as an intrinsic biomolecular carrier. To prove this concept, the phthalocyanine compounds were administered into SCC7 (squamous cell carcinoma) tumor-bearing mice via intravenous injection, and their biodistribution was monitored temporally by *in vivo* fluorescence imaging. As revealed in **Figure 4A-B** and **Figure S8**, all the compounds were shown to spread throughout the body immediately after injection and fade gradually with time, indicative of their efficient circulation in the blood stream. Concomitantly, they accumulated rapidly and stayed longer at the tumor site, allowing clear visualization of the tumor location *in vivo*. The biodistribution results determined by *ex vivo* imaging revealed that a significant amount of the phthalocyanine compounds were retained at the tumor site even at 7 d postinjection in spite of their rapid excretion from other parts of the body (**Figure 4C**). The consequent tumor-targeting ability is most likely attributable to the targeted transport by *in vivo* albumins via spontaneous binding of the phthalocyanines, where passive targeting would make an additional contribution in the case of dimer-binding ZnPcN$_4$ and ZnPcN$_{12}$ owing to the larger intrinsic carrier (albumin dimer, ~130 kDa), which can promote the size-dependent EPR effect. Efficient tumor accumulation of the phthalocyanines was also observed in a different type of tumor xenograft mouse model (HT-29, human colorectal adenocarcinoma), suggesting that the endogenous albumin-mediated delivery system can be a general strategy for systemic tumor targeting (**Figure S9**). Notably, methylene blue, a clinically used blue dye with negligible albumin-binding ability, did not show such tumor-targeting behavior upon systemic injection by itself (**Figure S10**), further corroborating that the spontaneous *in vivo* binding with albumin plays a crucial role in the tumor-targeting ability of our phthalocyanines.

PDT efficiency of the phthalocyanines in tumor-bearing mice

Encouraged by the *in vivo* tumor-targeting results, we next evaluated the phototherapeutic efficacy of these phthalocyanines by monitoring tumor growth inhibition after PDT treatment. To examine the effect of differently charged substituents, which were previously shown to determine the major binding partner (albumin monomer or dimer), we chose monomer-binding ZnPcS$_8$ and dimer-binding ZnPcN$_4$ for comparison and performed a single operation of PDT at 3 h postinjection, when the two compounds displayed similar levels of tumor accumulation (**Figure 4B**). In the operation, the phthalocyanines were intravenously injected into HT-29 tumor-bearing mice (tumor volume: 60-80 mm^3), and the tumors were exposed to red laser irradiation (655 nm, 200 mW, 30 min) at 3 h postinjection. As shown in **Figure 5A**, the mouse group treated with dimer-binding ZnPcN$_4$ presented apparent signs of tumor necrosis after PDT treatment, where the tumor surface manifested redness followed by scab formation within 5 d after PDT treatment. During the 2 week monitoring period, the tumor growth in that group was significantly suppressed, indicating successful PDT treatment with dimer-binding ZnPcN$_4$ (**Figure 5B**). In addition to its therapeutic efficacy, ZnPcN$_4$ caused no noticeable body weight loss in the treated mice, implying minimal toxic impacts on animal viability (**Figure 5C**). Interestingly, monomer-binding ZnPcS$_8$ did not show such a therapeutic effect even though its tumor accumulation level was observed to be similar to that of dimer-binding ZnPcN$_4$ in the *in vivo* and *ex vivo* images (**Figures 4B** and **S11**). In sharp contrast to the tumor inhibitory effect of ZnPcN$_4$, the group treated with ZnPcS$_8$ showed rapid tumor growth at a similar rate to that of the control group treated with PBS (pH 7.4), with no sign of tissue response to PDT (**Figure 5A-B**).

The distinct therapeutic responses observed above could be further confirmed by histological analysis of the tissue sections prepared from the tumors excised 1 d after each PDT treatment (**Figure 5D-E**). The tumor sections were stained for terminal deoxynucleotidyl transferase-mediated nick end labeling (TUNEL) and anti-Ki-67 immunohistochemical analyses, which allowed us to quantify the degree of apoptosis normalized by the degree of proliferation. It was observed that the tumor sections from the ZnPcN$_4$-treated group presented a 14-fold higher ratio of apoptosis index (TUNEL-positive cells)/proliferation index (Ki-67-positive cells) than those from the ZnPcS$_8$-treated group, evidencing the remarkably efficient phototherapy enabled by dimer-binding ZnPcN$_4$. These distinct PDT responses may be attributable to the different cell uptake efficiencies of phthalocyanines; i.e., in the presence of albumin-containing serum (FBS), highly negative

ZnPcS$_8$ exhibited the lowest cell uptake level and in turn the lowest PDT effect, whereas moderately positively charged ZnPcN$_4$ is superior in both cell uptake and phototoxicity while maintaining cell viability in the absence of light (**Figure 6**). Note that the PDT treatment with highly positive ZnPcN$_{12}$ caused severe pathological changes in the visceral organ tissues and that the mouse survival rate was decreased to zero at 3 d after PDT treatment, indicating acute toxicity (**Figure S12**). The *in vivo* toxicity of ZnPcN$_{12}$ is attributable to the highly

positively charged molecular structure [33,34] and the consequently strong dyeing effect on normal tissues around the tumor (**Figure 4**), which could cause collateral damage and toxicities when light diffuses through the tissue upon laser irradiation of the tumor. All these results suggest that among others, moderately positive dimer-binding ZnPcN$_4$ holds promise as an *in situ* albumin-binding photosensitizer for efficacious PDT of cancer by external carrier-free tumor targeting.
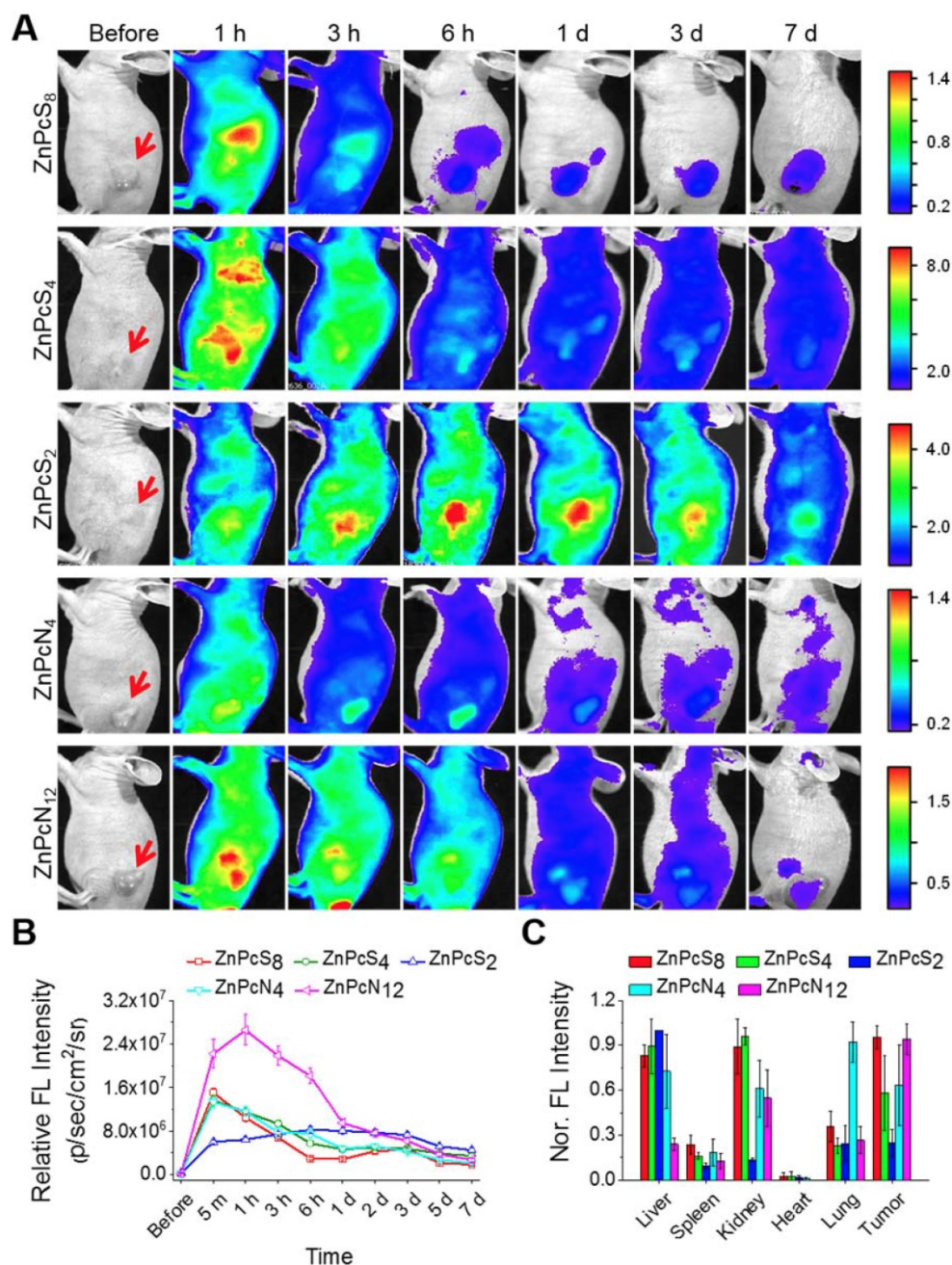

Figure 4. Biodistribution of the phthalocyanines in SCC-7 tumor-bearing mice. (A) *In vivo* fluorescence images of SCC7 tumor-bearing mice upon tail vein injection of the aqueous phthalocyanine solutions (200 µL, 200 µM). The red arrows indicate the tumor location. (B) Temporal tumor accumulation profiles of the phthalocyanines, as determined by fluorescence intensities from the tumor in *in vivo* images. (C) Biodistribution of the phthalocyanines, as determined *ex vivo* by fluorescence intensities from the tumor and other organs excised at 7 d postinjection.

Conclusion

In summary, we have developed five water-soluble phthalocyanines that show strong binding affinity for albumin. Interestingly, we found for the first time that the two positively charged compounds could selectively bind to albumin dimer over albumin monomer, while the three negatively charged phthalocyanines could bind to both albumin monomer and dimer. The binding modes of the phthalocyanines to HSA were well simulated, which should inspire increasing interest in the design and development of albumin monomer-targeted or albumin dimer-targeted probes or drug delivery strategies. Based on our interesting findings, we further demonstrated a green and efficient delivery approach using the native albumin *in vivo* as the carrier to enhance the tumor-targeting ability of these phthalocyanines. In particular, the phthalocyanine bearing four cationic groups, $ZnPcN_4$, displays outstanding PDT efficacy against tumors.
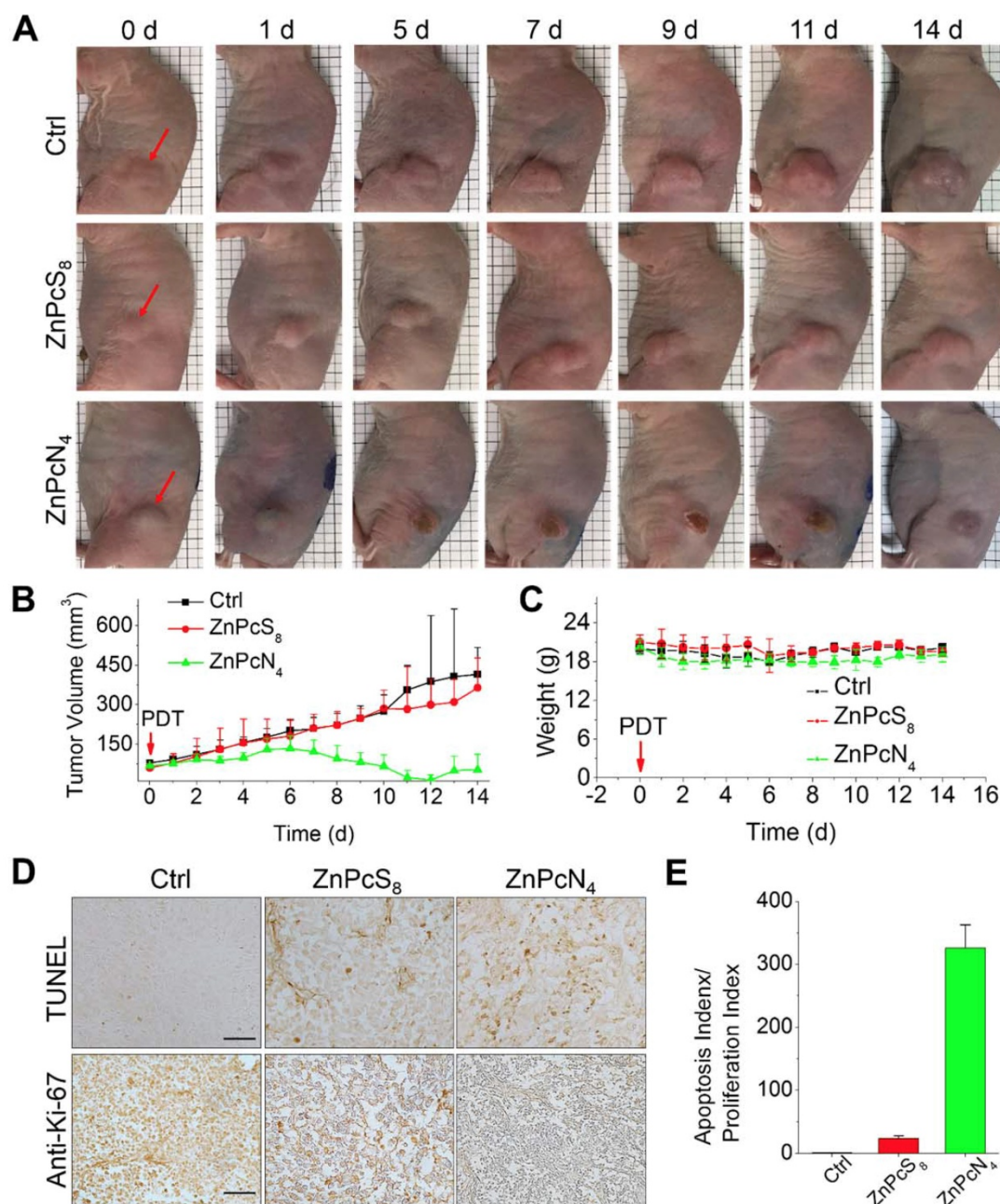

Figure 5. *In vivo* PDT treatment of HT-29 tumor-bearing mice with phthalocyanines. (A) Representative photographs of PDT-treated mice. For PDT treatment, laser irradiation (655 nm, 30 min) of the tumor tissue was performed at 3 h postinjection of the phthalocyanines (200 μL, 200 μM). In the control group, mice were exposed to laser irradiation after PBS (200 μL, pH 7.4) injection. The red arrows indicate the tumor location. (b-c) Temporal changes in tumor volume (B) and mouse body weight (C) during PDT treatments. (D) Histological images of tumor tissues resected from the mice 1 d after PDT treatment. Tumor sections were prepared for anti-Ki-67 immunohistochemical and TUNEL analyses. (E) Quantitative analysis of apoptosis and proliferation in tumor tissues. Apoptosis and proliferation indices were determined by the number of TUNEL- and Ki-67-positive cells in the histological images, respectively.
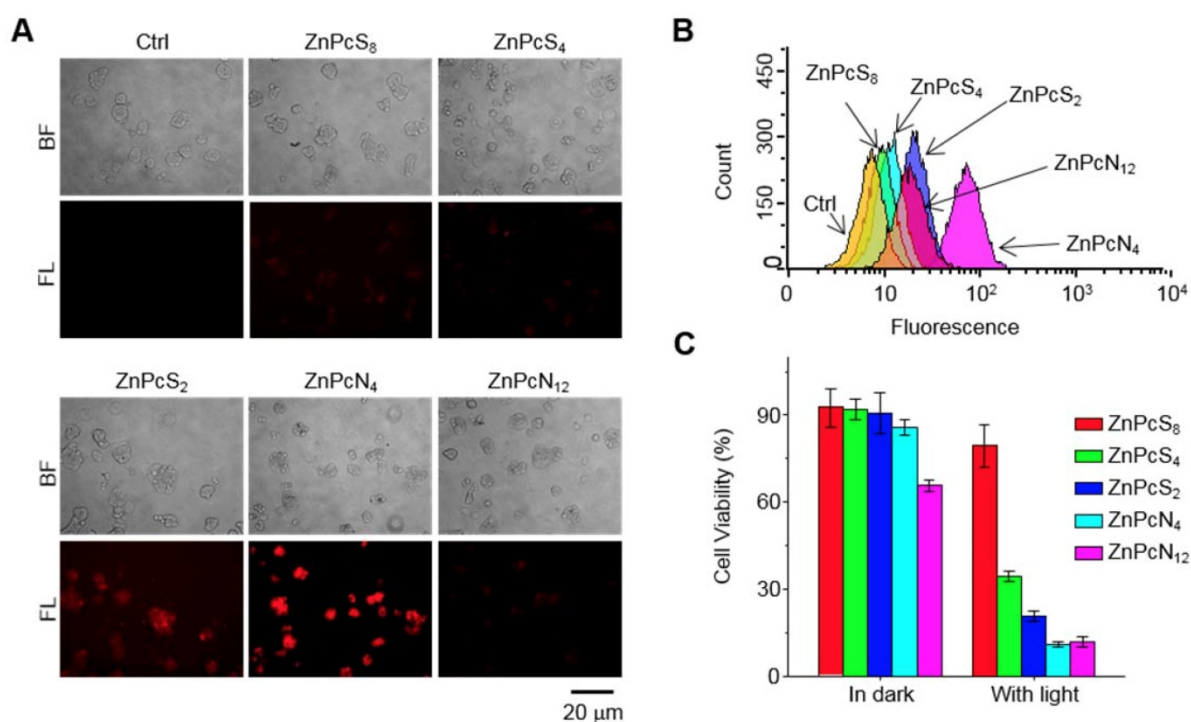
Figure 6. Intracellular delivery efficiency and photoinduced cytotoxicity of the phthalocyanines. (A-B) Fluorescence microscopic images (A) and flow cytometry analysis (B) indicating the uptake of phthalocyanines (20 μM) by HT-29 cells following 1 h of incubation. The images were obtained by using a filter set (excitation: 620 ± 30 nm, emission: 690 ± 30 nm). (C) Photoinduced cytotoxicity of phthalocyanines against HT-29 cells evaluated by the colorimetric MTT assay. Cells were exposed to laser irradiation (655 nm, 10 min) after intracellular delivery of the phthalocyanines.

Materials and Methods

Chemical materials and instruments. Methylene blue (MB), phthalonitrile, 1,8-diazabicyclo-[5.4.0]undec-7-ene (DBU), zinc acetate and BSA monomer were purchased from Sigma-Aldrich. $ZnPcS_8$, $ZnPcS_4$ and $ZnPcN_{12}$ were prepared using our previously described procedure [35-37]. The synthetic details of $ZnPcS_2$ and $ZnPcN_4$ are shown in the supplementary materials.

To obtain the BSA dimer/monomer (7/3) mixture, BSA (3.7 g, Sigma-Aldrich) in distilled water (70 mL) was incubated with Darco activated charcoal (3.5 g) washed with distilled water [38]. The BSA-charcoal mixture was titrated with 0.2 N HCl below pH 3.0 on ice. After incubation for 1 h, the supernatant was separated from the lipid-attached charcoal by centrifugation and was subsequently neutralized to pH 7.0 by adding 0.2 N NaOH. The lipid-free proteins were concentrated and then loaded onto a HiLoad 16/600 Superdex-75pg (GE Healthcare, USA) pre-equilibrated with A-buffer (50 mM Tris, 150 mM NaCl, pH 8.0). The fractions containing the BSA dimer/monomer mixture were collected and diluted 10-fold with B-buffer (50 mM Tris, pH 8.0). The diluted fraction was loaded onto a HiTrap Q Fast Flow (GE Healthcare, USA) pre-equilibrated with B-buffer. The BSA dimer/monomer mixture was eluted between 380 mM and 500 mM NaCl and

concentrated for loading onto a HiLoad 16/600 Superdex-200pg (GE Healthcare, USA) pre-equilibrated with A-buffer. The final BSA dimer/monomer fraction was concentrated to 27 mg/mL along with desalting against PBS buffer. The BSA dimer/monomer mixture was stored at -80 °C. During all purification procedures, the purity and homogeneity of the purified protein were determined based on native-PAGE analysis.

Electronic absorption spectra were recorded on a Shimadzu UV-2450 spectrophotometer. Fluorescence spectra were obtained on an Edinburgh FL900/FS900 spectrofluorometer.

Gel assays. The albumin-binding affinity of phthalocyanines was evaluated by gel retardation assay. For the experiments, a mixture of phthalocyanines (2 μM) and albumin (18 μM, a mixture of albumin monomer and albumin dimer) in PBS containing 10% DMSO was loaded onto a 10% native polyacrylamide (PAGE) gel, and electrophoresis was performed in Tris-glycine buffer solution at 110 V. After electrophoresis, CBB-stained albumin and phthalocyanine bands were visualized using a gel documentation system (Slimlight 5000K-M, Korea) and an IVIS Spectrum imaging system (PerkinElmer, USA), respectively. Furthermore, the mixture of phthalocyanines (2 μM) and FITC-labeled BSA monomer (18 μM) in PBS (pH 7.4) containing 10% DMSO was loaded onto 2%

agarose gel, and electrophoresis was performed in TAE buffer solution at 100 V. After electrophoresis, the gel was imaged using an IVIS spectrum imaging system.

Fluorescence titration. The binding constant of phthalocyanines with albumin was measured by fluorescence titration (Figure S6). The fluorescence spectra (excited at 280 nm) of albumin (3 μM) in water after adding different concentrations of phthlocyanines were measured. Then, their fluorescence intensity at 344 nm were recorded and used to calculated the binding constant according to the double logarithm regression curve, $Log((F_0-F)/F)=LogK+nLog[Pc]$ [39].

Computational studies. Protein and ligand preparations. The X-ray crystal structures of HSA complexed with heme molecule (PDB codes: 1N5U [40], 1O9X [41]) were prepared using the Protein Preparation Wizard in Maestro, version 9.2 (Schrödinger, LLC, NY, USA). During the preparation process, bond orders were assigned, hydrogen atoms were added, and protonation states of the residues at pH 7.4 were generated by Epik, version 2.6. All the hydrogen atoms were energy minimized with the optimized potential for liquid simulation (OPLS) 2005 force field until the average root-mean-square deviation (RMSD) for hydrogen atoms reached 0.30 Å. Since the metal-coordinated ligand molecule cannot be appropriately prepared with the conventional ligand preparation tool, metal coordination in the phthalocyanine molecule was prepared using the Protein Preparation Wizard. The resulting structures were energy minimized using the implicit solvent and OPLS 2005 force fields.

Blind docking and binding mode selection. The ligands were docked into several binding pockets of HSA with Glide, version 6.1, in Maestro using the following steps: (i) Initially, the grid box was generated using the centroid of the cocrystallized ligand. We set the grid box size large enough to cover all the binding cavities in HSA. (ii) For the docking stage, Glide SP (standard precision) docking, which searches for up to 500 conformations per ligand, was performed. (iii) The docked conformations were clustered based on their RMSDs, and the final modes were selected based on their scores and populations.

Dimer modeling. The positively charged compounds were docked to the HSA monomer first, and then the dimer model was generated using the available HSA homodimer crystal structure complexed with lidocaine (PDB code: 3JQZ) [32]. Since this crystal structure's binding site is too small relative to our compound, the original docking to the PDB structure (3JQZ) failed to retrieve the solution. The complex structure of ZnPcN$_4$ and HSA monomer was aligned to the dimer crystal structure, and then the monomer model and the ligand-free dimer partner (chain B) of 3JQZ.pdb were merged. The merged chain B was further refined using energy minimization and MC sampling. The OPLS3 force field [42] and the variable-dielectric generalized Born (VSGB) solvation model were used during the simulation. After 10000 steps of MC sampling, the lowest energy model structure was obtained.

All computational studies were undertaken on an Intel Xeon octa-Core 2.5 GHz workstation with Linux CentOS, release 5.8, and the molecular graphics figures were generated by PyMOL software (http://www.pymol.org).

Intracellular delivery into cancer cells. HT-29 cells were seeded onto 35-mm cover glass bottom dishes (1×10^5 cells per dish). Once they reached a confluence of 70-80%, cells were washed twice with PBS (pH 7.4) and treated with phthalocyanines (20 μM in RPMI 1640 medium). After 1 h of incubation, the cells were washed twice with PBS (pH 7.4) and recharged with fresh media. Cells were imaged by using a LEICA DMI3000B fluorescence microscope equipped with a Nuance FX multispectral imaging system (CRI, USA).

To quantitatively evaluate the intracellular delivery efficiency, HT-29 cells were seeded on 6-well plates (1×10^6 cells per well). After 24 h of incubation, the cells were treated with phthalocyanines (20 μM in RPMI 1640 medium) for 1 h. Then, the cells were washed twice with PBS (pH 7.4), trypsinized, and collected by centrifugation. The collected cells were analyzed by a Guava easyCyteTM flow cytometer (EMD Millipore, USA).

Photo-induced cytotoxicity against cancer cells. HT-29 cells were seeded in 96-well plates (1×10^4 cells per well). Once they reached a confluence of 70-80%, the cells were treated with phthalocyanines (20 μM in RPMI1640 medium). After 1 h of incubation, the cells were recharged with fresh media, exposed to laser irradiation (655 nm, 200 mW, 10 min), and further incubated for 24 h. Cell viability was evaluated via the colorimetric MTT assay [43].

In vivo **and** *ex vivo* **imaging of tumor accumulation.** The animal study was performed according to the guidelines offered by the Korea Institute of Science and Technology (KIST). For animal experiments, BALB/c nude mice (5-week-old male; Orient Bio Inc., Korea) were anesthetized with intraperitoneal injection of a mixture of Zoletil-Rompun. Tumors were established by subcutaneous inoculation of SCC7 (1×10^6 cells in 60 μL of culture medium) or HT-29 (1×10^7 cells in 100 μL of culture medium) cells into mice. All *in vivo* fluorescence images were taken at designated time

points for 1 week after intravenous injection of the aqueous phthalocyanine solution (200 μL, 200 μM) with an IVIS Spectrum imaging system. For *ex vivo* fluorescence imaging, organs including tumors were excised at 7 d postinjection of the phthalocyanines from mice and imaged with an IVIS Spectrum imaging system.

***In vivo* photodynamic therapy.** The aqueous phthalocyanine solution (200 μL, 200 μM) was intravenously injected into HT-29 tumor xenograft mice (n = 4 per group). At 3 h postinjection, tumors were exposed to laser irradiation at 655 nm for 30 min. The tumor volumes were measured and calculated with a × b^2/2, where a and b are the largest and smallest diameters of the tumor, respectively. For histological examination, tumors were excised from the mice 1 d after PDT treatment with phthalocyanines to be fixed in neutral buffered formalin and embedded in paraffin. The tissue blocks were cut into 10 μm sections and stained for anti-Ki-67 immunohistochemical and terminal deoxynucleotidyl transferase-mediated nick end labeling (TUNEL) analyses. Proliferation and apoptosis indices were determined by quantitation of Ki-67- and TUNEL-positive cells, respectively [44].

Evaluation of biocompatibility. For the *in vivo* toxicity study, the visceral organs were excised 1 d after PDT treatment with phthalocyanines. The tissue blocks of the organs were prepared according to the same procedure as the one explained above for tumor block preparation, and hematoxylin (H) and eosin (E) staining was performed to assess the extent of the pathological changes. Photomicrographs of tissue sections were acquired using an Olympus BX51 microscope and image transfer software (Olympus, Tokyo, Japan).

Supplementary Material

Supplementary figures and the synthesis procedures of the compounds.

http://www.thno.org/v09p6412s1.pdf

Acknowledgements

Author contributions

X.L. conceived of the idea, synthesized the phthalocyanines, performed the optical spectrum detections, analyzed the data, and wrote the manuscript. S.K. performed the gel assays, *in vitro* and *in vivo* fluorescence imaging and PDT evaluations. Y.L. designed and performed the computational simulations, and participated in the writing of manuscript. T.G. assisted the analysis of data and the preparation of manuscript. D.L., J.P. and N.K. assisted the gel assays and in vivo tests. J. H. N., S. K. H., and S. S. C. prepared the BSA dimer/monomer (7/3) mixture and performed one of the gel assay as shown in Figure S1. All authors commented on the manuscript. J.D.H. supervised the synthesis of the phthalocyanines and revised the manuscript. S.C. supervised the computational studies and revised the manuscript. S.K. supervised the gel assays and *in vivo* tests, and revised the manuscript. J.Y. supervised all the studies and revised the manuscript.

Competing Interests

The authors have declared that no competing interest exists.

References

1. Sawyers C. Targeted cancer therapy. Nature. 2004; 432: 294-297.
2. Biankin AV, Piantadosi S, Hollingsworth SJ. Patient-centric trials for therapeutic development in precision oncology. Nature. 2015; 526: 361-370.
3. von Maltzahn G, Park JH, Lin KY, Singh N, Schwöppe C, Mesters R, et al. Nanoparticles that communicate in vivo to amplify tumour targeting. Nat Mater. 2011; 10: 545-552.
4. Dewhirst MW, Secomb TW. Transport of drugs from blood vessels to tumour tissue. Nat Rev Cancer. 2017; 17: 738-750.
5. Rosenblum D, Joshi N, Tao W, Karp JM, Peer D. Progress and challenges towards targeted delivery of cancer therapeutics. Nat Commun. 2018; 9: 1410.
6. Liu Q, Chen X. Simple bioconjugate chemistry serves great clinical advances: albumin as a versatile platform for diagnosis and precision therapy. Chem Soc Rev. 2016; 45: 1432-1456.
7. Chen Q, Liu Z. Albumin carriers for cancer theranostics: a conventional platform with new promise. Adv Mater. 2016; 28: 10557-10566.
8. Stehle G, Sinn H, Wunder A, Schrenk HH, Stewart JCM, Hartung G, et al. Plasma protein (albumin) catabolism by the tumor itself-implications for tumor metabolism and the genesis of cachexia. Crit Rev Oncol Hematol. 1997; 26: 77-100.
9. Tiruppathi C, Song W, Bergenfeldt M, Sass P, Malik AB. Gp60 activation mediates albumin transcytosis in endothelial cells by tyrosine kinase-dependent pathway. J Biol Chem. 1997; 272: 25968-25975.
10. Lin T, Zhao P, Jiang Y, Tang Y, Jin H, Pan Z, et al. Blood-brain-barrier-penetrating albumin nanoparticles for biomimeric drug delivery via albumin-binding protein pathways for antiglioma therapy. ACS Nano. 2016; 10: 9999-10012.
11. Zhu G, Lynn GM, Jacobson O, Chen K, Liu Y, Zhang H, et al. Albumin/vaccine nanocomplexes that assemble in vivo for combination cancer immunotherapy. Nat Commun. 2017; 8: 1954.
12. Guo L, Luo S, Du Z, Zhou M, Li P, Fu Y, et al. Targeted delivery of celastrol to mesangial cells is effective against mesangioproliferative glomerulonephritis. Nat Commun. 2017; 8: 878.
13. Zheng YR, Suntharalingam K, Johnstone TC, Yoon H, Lin W, Brooks JG, et al. Pt(IV) prodrugs designed to bind non-covalently to human serum albumin for drug delivery. J Am Chem Soc. 2014; 136: 8790-8798.

14. Jin C, Zhang H, Zou J, Liu Y, Zhang L, Li F, et al. Fluoxuridine homomeric oligonucleotides "hitchhike" with albumin in situ for cancer chemtherapy. Angew Chem Int Ed. 2018; 57: 1-5.

15. Chen Z, Liu L, Liang R, Luo Z, He H, Wu Z, et al. Biosinspired hybrid protein oxygen nanocarrier amplified photodynamic therapy for eliciting anti-tumor immunity and abscopal effect. ACS Nano. 2018; 12: 8633-8645.

16. Li Z, Hu Y, Howard KA, Jiang T, Fan X, Miao Z, et al. Multifunctional bismuth selenide nanocomposites for antitumor thermo-chemotherapy and imaging. ACS Nano. 2016; 10: 984-997.

17. Li X, Zheng BD, Peng XH, Li SZ, Ying JW, Zhao Y, et al. Phthalocyanines as medicinal photosensitizers: developments in the last five years. Coord Chem Rev. 2019; 379: 147-160.

18. Li X, Kolemen S, Yoon J, Akkaya EU. Activatable photosensitizers: agents for selective photodynamic Ttherapy. Adv Funct Mater. 2017; 27: 1604053.

19. Li X, Lee S, Yoon J. Supramolecular photosensitizers rejuvenate photodynamic therapy. Chem Soc Rev. 2018; 47: 1174-1188.

20. Li X, Kim CY, Lee S, Lee D, Chung HM, Kim G, et al. Nanostructured phthalocyanine assemblies with protein-driven switchable photoactivities for biophotonic imaging and therapy. J Am Chem Soc. 2017; 139: 10880-10886.

21. Li X, Lee D, Huang JD, Yoon J. Phthalocyanine-assembled nanodots as photosensitizers for highly efficient type I photoreactions in PDT. Angew Chem Int Ed. 2018; 57: 9885-9890.

22. Li R, Zheng K, Hu P, Chen Z, Zhou S, Chen J, et al. A novel tumor targeting drug carrier for optical imaging and therapy. Theranostics. 2014; 4: 642-659.

23. Li X, Kim CY, Shin JM, Lee D, Kim G, Chung HM, et al. Mesenchymal stem cell-driven activatable photosensitizers for precision photodynamic oncotherapy. Biomaterials. 2018; 187: 18-26.

24. Lan WL, Liu FR, Ke MR, Lo PC, Fong WP, Ng DKP, et al. The effects of formulation and serum albumin on the in vitro photodynamic activity of zinc(II) phthalocyanines substituted with sulfonated quinolineoxy groups. Dyes Pigm. 2016; 128: 215-225.

25. Majorek KA, Porebski PJ, Dayal A, Zimmerman MD, Jablonska K, Stewart AJ, et al. Structural and immunologic characterization of bovine, horse, and rabbit serum albumins. Mol Immunol. 2012; 52: 174-182.

26. dos Remedios CG, Moens PD. Fluorescence resonance energy transfer spectroscopy is a reliable "ruler" for measuring structural changes in proteins: dispelling the problem of the unknown orientation factor. J Struct Biol. 1995; 115: 175-185.

27. Taguchi K, Chuang VT, Maruyama T, Otagiri M. Pharmaceutical aspects of the recombinant human serum albumin dimer: structural characteristics, biological properties, and medical applications. J Pharm Sci. 2012; 101: 3033-3046.

28. Richard MJ, Arnaud J, Jurkovitz C, Hachache T, Meftahi H, Laporte F, et al. Trace elements and lipid peroxidation abnormalities in patients with chronic renal failure. Nephron. 1991; 57: 10-15.

29. Scorza G, Minetti M. One-electron oxidation pathway of thiols by peroxynitrite in biological fluids: Bicarbonate and ascorbate promote the formation of albumin disulphide dimers in human blood plasma. Biochem J.1998; 329: 405-413.

30. Mimic-Oka J, Simic T, Djukanovic L, Reljic Z, Davicevic Z. Alteration in plasma antioxidant capacity in various degrees of chronic renal failure. Clin Nephrol. 1999; 51: 233-241.

31. Ogasawara Y, Namai T, Togawa T, Ishii K. Formation of albumin dimers induced by exposure to peroxides in human plasma: A possible biomarker for oxidative stress. Biochem Biophys Res Commun. 2006; 340: 353-358.

32. Hein KL, Kragh-Hansen U, Morth JP, Jeppesen MD, Otzen D, Moller JV, et al. Crystallographic analysis reveals a unique lidocaine binding site on human serum albumin. J Struct Biol. 2010; 171: 353-360.

33. Moghimi SM, Symonds P, Murray JC, Hunter AC, Debska G, Szewczyk A. A two-stage poly(ethylenimine)-mediated cytotoxicity: implications for gene transfer/therapy. Mol Ther. 2005; 11: 990-995.

34. Peng L, Gao Y, Xue YN, Huang SW, Zhuo RX. Cytotoxicity and in vivo tissue compatibility of poly(amidoamine) with pendant aminobutyl group as a gene delivery vector. Biomaterials. 2010; 31: 4467-4476.

35. Li XS, Ke MR, Zhang MF, Tang QQ, Zheng BY, Huang JD. A non-aggregated and tumour-associated macrophage-targeted photosensitizer for photodynamic therapy: a novel zine(II) phthalocyanine containing octa-sulphonates. Chem Commun. 2015; 51: 4704-4707.

36. Li XS, Ke MR, Huang W, Ye CH, Huang JD. A pH-responsive layered double hydroxide (LDH)-phthalocyanine nanohybrid for efficient photodynamic therapy. Chem Eur J. 2015; 21: 3310-3317.

37. Li XS, Guo J, Zhuang JJ, Zheng BY, Ke MR, Huang JD. Highly positive-charged zinc(II) phthalocyanine as non-aggregated and efficient antifungal photosensitizer. Bioorg Med Chem Let. 2015; 25: 2386-2389.

38. Chen RF. Removal of fatty acids from serum albumin by charcoal treatment. J Biol Chem. 1967; 242: 173-181.

39. Liu Y, Xie MX, Jiang M, Wang YD. Spectroscopic investigation of the interaction between human serum albumin and three organic acids. Spectrochim Acta, Part A. 2005; 61: 2245-2251.

40. Wardell M, Wang Z, Ho JX, Robert J, Ruker F, Ruble J, et al. The atomic structure of human methemalbumin at 1.9 A. Biochem Biophys Res Commun. 2002; 291: 813-819.

41. Zunszain PA, Ghuman J, Komatsu T, Tsuchida E, Curry S. Crystal structural analysis of human serum albumin complexed with hemin and fatty acid. BMC Struct Biol. 2003; 3: 6.

42. Harder E, Damm W, Maple J, Reboul M, Xiang JY, Wang L, et al. OPLS3: A force field providing broad coverage of drug-like small molecules and proteins. J Chem Theory Comput. 2016; 12: 281-296.

43. Mosmann T. Rapid colorimetric assay for cellular growth and survival: application to proliferation and cytotoxicity assays. J Immunol Methods. 1983; 65: 55-63.

44. Burtrum D, Zhu Z, Lu D, Anderson DM, Prewett M, Pereira DS, et al. A fully human monoclonal antibody to the insulin-like growth factor I receptor blocks ligand-dependent signaling and inhibits human tumor growth in vivo. Cancer Res 2003; 63: 8912-8921.